RESEARCH/REVIEW ARTICLE

Late Holocene climate change recorded in proxy records from a Bransfield Basin sediment core, Antarctic Peninsula

Alex Barnard,[1] Julia S. Wellner[1] & John B. Anderson[2]

[1] Department of Earth and Atmospheric Sciences, University of Houston, 4800 Calhoun Road, Houston, TX 77204, USA
[2] Department of Earth Science, Rice University, MS-126, 6100 Main Street, Houston, TX 77005, USA

Keywords
Antarctic Peninsula; palaeoclimate; Holocene; marine; isotopes.

Correspondence
Alex Barnard, Department of Earth and Atmospheric Sciences, University of Houston, 4800 Calhoun Road, Houston, TX 77204, USA.
E-mail: abarnard2@uh.edu

Abstract

The glacimarine environment of the Antarctic Peninsula region is one of the fastest warming places on Earth today, but details of changes in the recent past remain unknown. Large distances and widespread variability separate late Holocene palaeoclimate reconstructions in this region. This study focuses on a marine sediment core collected from ca. 2000 m below sea level in the Central Bransfield Strait that serves as a key for understanding changes in this region. The core yielded a high sedimentation rate and therefore provides an exceptional high-resolution sedimentary record composed of hemipelagic sediment, with some turbidites. An age model has been created using radiocarbon dates that span the Late Holocene: 3560 cal yr BP to present. This chronostratigraphic framework was used to establish five units, which are grouped into two super-units: a lower super-unit (3560–1600 cal yr BP) and an upper super-unit (1600 cal yr BP–present), based on facies descriptions, laser particle size analysis, x-ray analysis, multi-sensor core logger data, weight percentages and isotopic values of total organic carbon and nitrogen. We interpret the signal contained within the upper super-unit as an increase in surface water irradiance and/or shortening of the sea-ice season and the five units are broadly synchronous with climatic intervals across the Antarctic Peninsula region. While the general trends of regional climatic periods are represented in the Bransfield Basin core we have examined, each additional record that is obtained adds variability to the known history of the Antarctic Peninsula, rather than clarifying specific trends.

The Antarctic Peninsula is a rapidly warming region that encompasses both marine and glacial environments. Records spanning the past 50 years from the Antarctic Peninsula show a temperature increase of 0.56°C per decade when averaged over the year, and an increase of 1.09°C per decade in the austral winter months, compared to the global mean of 0.13°C ± 0.03 per decade (Turner et al. 2005). Austral winter temperatures in parts of the Antarctic Peninsula region have risen by about 6°C over the past 50 years. In addition, in recent years the western Antarctic Peninsula region has experienced more intense ocean warming than the global average, more than 1°C since 1950, as well as increased salinity, in the upper 100 m (Meredith & King 2005). Thus current warming across the Antarctic Peninsula region is unusual in both synchronicity and extent (e.g., Cook et al. 2005; Steig et al. 2009; Mulvaney et al. 2012). This contrasts with published palaeoclimate records taken from marine sediment cores that document diachronous climatic change throughout the Holocene. An understanding of the historical context of this rapid, regional climate change is necessary for the development of models of future changes. To elucidate the Late Holocene climatic changes occurring in different parts of the Bransfield Basin, and their relationships to one another, this study compares new data from a central position in the region with four marine-based sedimentary records derived from similar methods (Domack et al. 2001; Heroy et al. 2008; Michalchuk et al. 2009; Milliken et al. 2009) (Fig. 1).

Citation: *Polar Research* 2014, *33*, 17236, http://dx.doi.org/10.3402/polar.v33.17236

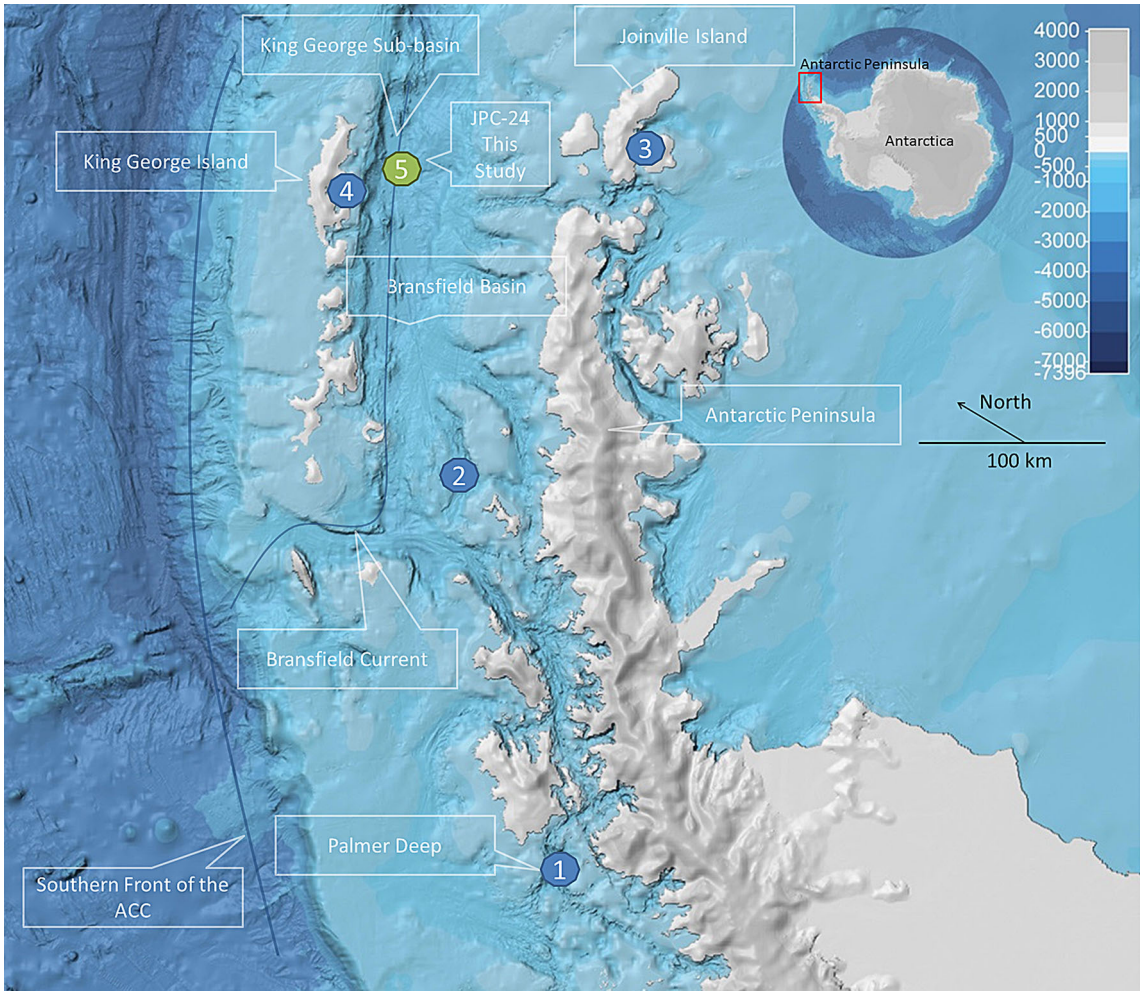

Fig. 1 Inset shows the location of the Antarctic Peninsula. Main figure is a regional map of the western Antarctic Peninsula study area including multibeam bathymetry from the International Bathymetric Chart of the Southern Ocean (Arndt et al. 2013), created using Fledermaus software (Quality Positioning Systems BV, Zeist, Netherlands). The location of the Antarctic Circumpolar Current (ACC) and Bransfield Current are shown. Four study sites with published records that data in this study are compared to are as follows: (1) Domack et al. (2001); (2) Heroy et al. (2008); (3) Michalchuk et al. (2009); and (4) Milliken et al. (2009) and Majewski et al. (2012). This study (5) is the site of core JPC-24, collected during NBP0703.

Environmental setting

The Antarctic Peninsula is the warmest and wettest part of Antarctica. Storms, generated in the Amundsen Sea, track into the Bellingshausen Sea, deflect north along the Antarctic Peninsula, and eventually reach the Scotia Sea. Because of these storms, the western/northern seaboard of the Antarctic Peninsula has a comparatively warm, humid climate. In comparison, the eastern side is colder and drier (Reynolds 1981). The dominant controls of temperature and precipitation patterns across the peninsula are storms and orographic effects. Temperature differences between the north and south are controlled by latitudinal temperature gradients. Temperature data from across the Antarctic Peninsula (Reynolds 1981; Vaughan & Doake 1996) document a broad, regional, thermal control of ice shelves on the western Antarctic Peninsula. Ice shelves exist only on the cold side of the -5 to -9°C isotherm (Vaughan & Doake 1996). Moreover, temperature changes affect glacial sediment yields as shown by recent increases in sediment accumulation rates from the Antarctic Peninsula to Patagonia (Boldt et al. 2013).

The source of coastal waters in Antarctica is the mid-level water mass of the Antarctic Circumpolar Current, which is composed of warm, saline, Circumpolar Deep Water. Circumpolar Deep Water is divided into upper and lower units, with the Upper Circumpolar Deep Water distinguished by its relatively warm temperature and the

Citation: *Polar Research* 2014, *33*, 17236, http://dx.doi.org/10.3402/polar.v33.17236

Lower Circumpolar Deep Water by its relatively high salinity. The Antarctic Circumpolar Current bifurcates around the South Shetland Islands and traverses the length of the northern Bransfield Strait as the Bransfield Current (Meredith et al. 2010), and has in recent years provided regular intrusions of Upper Circumpolar Deep Water onto the continental shelf (Ducklow et al. 2007). This is important because the Upper Circumpolar Deep Water is 3–4°C above freezing, significantly warmer than the Bransfield Strait water temperature that varies seasonally between 0 and −2°C in the austral summer and winter, respectively. In this region, where the average thickness of sea ice is less than 1 m, a 1°C increase in surface ocean temperature is equivalent to a 30 cm reduction in the formation of sea ice (Meredith & King 2005). The presence of Upper Circumpolar Deep Water has also been associated with increases in productivity (Prezelin et al. 2000).

Since the Last Glacial Maximum, when grounded ice reached the continental shelf and perennial sea ice covered the Bransfield Strait (Heroy & Anderson 2005, 2007; Simms et al. 2011), ice has continued to retreat with some minor re-advances. Bentley et al. (2009) provide a synthesis of the Holocene climate and outline five periods. Three warm periods (Mid-Holocene Warm Period, Medieval Warm Period and the recent rapid warming) that are associated with warmer ocean waters, higher productivity and higher sedimentation rates. Two intervening cold periods (Neoglacial and Little Ice Age) are associated with intense perennial sea ice and colder air temperatures. Climate controlled the sedimentary evolution of the western Antarctic Peninsula throughout the Holocene, regionally determining the pattern and volume of sediment delivery and facies variability (Griffith & Anderson 1989). The present-day synchronous rapid warming of the Antarctic Peninsula contrasts with published Holocene marine sediment core records that document diachronous climatic changes across the region (Domack et al. 2001; Heroy et al. 2008; Michalchuk et al. 2009; Milliken et al. 2009; Majewski et al. 2012). Palaeoenvironmental proxy data in these studies shows that Late Holocene climate change was broadly synchronous in extent, although the timing varied with latitude and location. Published proxy records suggest that the onset of the Neoglacial varies with distance from the continent, occurring earlier in the sites closest to the Antarctic Peninsula and later in the more northerly sites (Domack et al. 2001; Taylor & Sjunneskog 2002; Heroy et al. 2008; Michalchuk et al. 2009; Milliken et al. 2009). The existence of a Medieval Warm Period and a Little Ice Age in Antarctica is uncertain since each has been documented in only a few records (Bentley et al. 2009).

Study area

The study area is the Bransfield Strait in the northwestern Antarctic Peninsula (Fig. 1). This area lies adjacent to the most northerly part of the Antarctic continent, and extends north into the Southern Ocean to 63°S. Along the northern continental margin of the Antarctic Peninsula lie the South Shetland Islands. These islands are separated from the Antarctic Peninsula by the Bransfield Strait, a distance of about 125 km (Fig. 1). The strait opens in the west to the Bellingshausen Sea and in the east to the Weddell Sea and is the geographic counterpart of the geologic Bransfield Basin. The basin is further subdivided into three domains: the West Bransfield Basin, the Central Bransfield Basin and the East Bransfield Basin. The flat-bottomed part of the Central Bransfield Basin adjacent to King George Island is known as the King George Sub-basin.

Methods

The data used in this study were collected in 2007 onboard the RV/IB *Nathaniel B. Palmer*, during cruise NBP0703. Real-time geophysical data were analysed onboard and used to identify a coring location in the King-George Sub-basin of the Central Bransfield Basin where undisturbed hemipelagic sediment would be sampled (García et al. 2008). Jumbo piston core JPC-24 (22 m) and Jumbo trigger core JTC-24 (1.33 m) were recovered from a water depth of 1980 m (62° 16.449′S, 57° 38.7000′W; Fig. 2). A hull mounted Bathy 2000 (Ocean Data Equipment Corporation, Warwick, RI, USA) unit

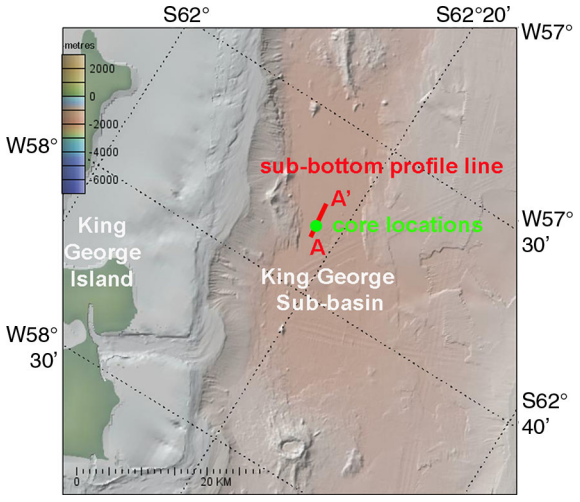

Fig. 2 Bathymetry of the Bransfield Basin. Location of Fig. 3 is shown as a red line with core locations as a green circle. Map created using GeoMapApp (Carbotte et al. 2007).

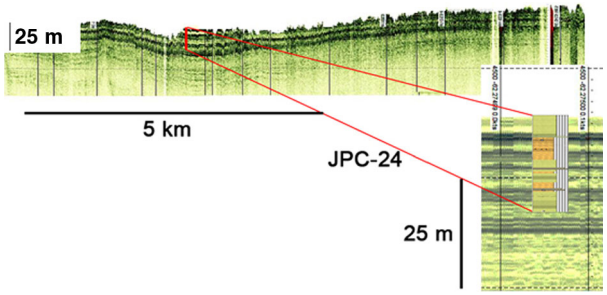

Fig. 3 Chirp 3.5 kHz sub-bottom profile, y-axis is depth and x-axis is distance. Vertical exaggeration in the bathymetric profile is approximately 40. Inset: changes in the core lithology (JPC-24) correlate with acoustic reflection surfaces. The location is shown in Fig. 2. Inset: core lithology represented by colours, where green is clayey mud, orange is clay, grey is sand–gravel and mottling represents abundant organic matter. Vertical bars are grain size, from left to right: clay, sand, gravel.

with a 3.5 kHz swept frequency source was used in conjunction with an EM120 multibeam unit (Simrad, Horten, Norway) to provide a detailed image of the seafloor and upper sediment layers (Figs. 2, 3). In the onboard laboratory, detailed sediment core analyses were completed including: colour (using a Munsell colour chart), grain size and sedimentary and biogenic structures. The core was also digitally recorded using a camera and then sampled for a preliminary study of the sediment composition.

Radiocarbon dates

Seven carbonate samples collected from the core were sent to the University of California Irvine for accelerated mass spectrometry dating. The CALIB V.6 software program was used for calibration and correction (Stuiver et al. 2005). A ΔR of 700 years was added to the standard marine reservoir correction of about 350–400 years, giving the 1100-year correction appropriate for Antarctic waters (Domack et al. 2001; Milliken et al. 2009). The dates are provided in Table 1.

Sedimentology

The sediment cores were described as part of NBP0703 and detailed facies descriptions, and sampling intervals were conducted at the Antarctic Research Facility, Florida State University. The core contains four main facies that include green silty clay, dark olive grey silt, very poorly sorted sand and clay and fining upwards sandy layers. Sediment magnetic susceptibility and density were recorded at 1 cm intervals using an MSCL 7.6 (Geotek, Deventry, UK). Artefacts caused both by division of the core into individual sections and zones of incomplete core recovery have been removed from the data. Additional samples were collected for laser particle size analysis at 10 cm intervals. Measurements were conducted using a Mastersizer 2000 (Malvern Instruments, Worcester, UK). Magnetic susceptibility is used to estimate relative abundance of terrigenous versus biogenic material following Anderson (1999). X-ray radiographs were supplied by the Antarctic Research Facility at a 1:1 scale at 300 dpi, used as a non-invasive techniques to find pebbles (>4 mm) down core at 5 cm intervals.

Geochemistry

For geochemical analysis, we collected 107 samples. Samples (10 cc) were taken at 20 cm intervals down core, in 1 cm diameter sample tubes. Sample preparation followed methods outlined in Milliken et al. (2009). Samples were analysed at the University of California Davis. Isotopic values and elemental values of carbon and nitrogen were measured using continuous flow mass spectrometry. Precision of the measurements is $\pm 0.1‰$ for isotopic values (δ) of carbon, $\pm 0.2‰$ for nitrogen,

Table 1 Dates were calibrated using Calib v.6.0 software and using the marine 04.14c calibration curve that incorporates a 350–400 years correction (Stuiver et al. 2005). A marine reservoir ΔR of 700 years was added, making the total marine reservoir correction about 1100 years.

Lab. no.	Core depth (cm)	Fraction modern (‰)	±	$\delta^{14}C$ (‰)	±	^{14}C age (BP)	±	Cal yr BP	±[a]
69391	0[b]	0.87	0.0013	−126	1.3	1080	15	−57[d]	2
69389	490[c]	0.76	0.0013	−242	1.3	2225	15	1081	37
40843	556[c]	0.78	0.0021	−219	2.1	1985	25	832[d]	44
69390	671[b]	0.75	0.0010	−254	1.0	2360	15	1228	32
40852	1273[c]	0.70	0.0021	−300	2.1	2865	25	1759[d]	43
40850	1692	0.63	0.0017	−368	1.7	3680	25	2750	11
40853	2194[c]	0.58	0.5821	−418	6.2	4350	90	3559[d]	54

[a]1σ error of calibrated age.
[b]From articulated shells.
[c]From shell fragment material.
[d]Dates used in the radiocarbon age model.

Citation: *Polar Research* 2014, *33*, 17236, http://dx.doi.org/10.3402/polar.v33.17236

0.5% for carbon (μg), and 0.1% for nitrogen (μg). Organic carbon and nitrogen results were normalized using the weight of sediment (μgC, N/sediment weight [μg]) to give weight percentages (wt.%). The isotopic values were supplied by the University of California Davis in parts per thousand (‰), relative to Pee Dee Belemnite (PDB) (carbon) and air (nitrogen). We have adapted the calculation of mass accumulation rates from Willmott et al. (2009) that uses the elemental concentration of carbon and nitrogen, dry bulk density and sedimentation rate to calculate organic matter mass accumulation rates by removing dry bulk density. Including dry bulk density as calculated from multi-sensor core logger density does not change the mass accumulation rates significantly and it is therefore omitted allowing use of the equation over a broader range of data sets. The equation we use is:

$$\text{Mass accumulation rate}_{(\text{TOC, N})} = \frac{\text{TOC, N (wt\%)}}{100 \cdot \text{sedimentation rate (cm yr}^{-1})} \quad (1)$$

Results

Geophysical analysis and core integration

Core JPC-24 and JTC-24 were recovered from the 2000 m deep King George Sub-basin. The core is mostly composed of green-grey diatomaceous silty clays and clayey silt. Continuous parallel reflections in the sub-bottom profile correlate with the JPC-24 core lithology, suggesting the complete recovery of recent sediments. Results from a trigger core (JTC-24) taken at the same location corroborate the integrity of the core top.

Radiocarbon age model

The highest stratigraphic date was recovered from 0 cm and yielded an age of 0 calibrated years before present (cal yr BP; laboratory number 69391; Table 1). Since it is difficult to use radiocarbon dating techniques on material younger than 1950, we set our 0 cal yr BP date to represent the most recent sediment, and acknowledge that this tallies with our linear age model. A simple linear interpolation age model has been constructed for the youngest radiocarbon dates (Fig. 4) and is used to convert depth in core (cm) to cal yr BP. Of the seven carbonate samples dated we chose the four youngest dates to construct an age model for this core, including the core-top zero date. Three older dates that do not fall in chronological order, along a linear regression of the youngest dates, are only older by a few hundred years and reinforce the existing age model, providing a possible age range for delivery of reworked sediments to the deep Bransfield Basin.

Super-units and units

According to our age model we present two super-units and five units that have been recognized based on facies analysis, grain size data, magnetic susceptibility, pebble count, and weight percentages, ratio and isotopic values of carbon and nitrogen (Fig. 5). For the whole data set,

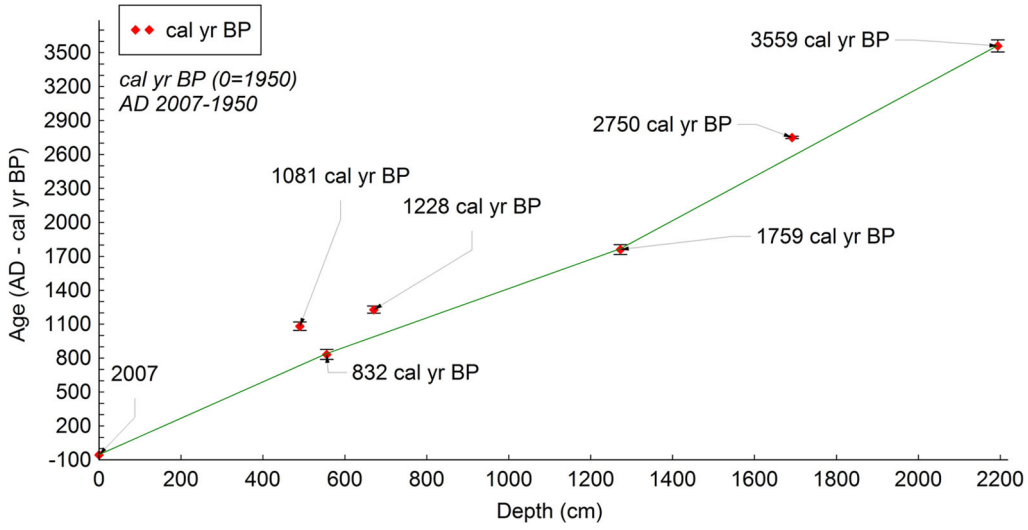

Fig. 4 Age model for the radiocarbon dates, constructed by linear interpolation, showing 1σ error bars. Because 1950 AD is equivalent to 0 cal yr BP, the age model uses negative values on the x axis to reach 2007 AD (−57 cal yr BP). The calculated sedimentation rate, based on a linear interpretation from the origin to 22 m at 3559 cal yr BP, is 0.6 cm/yr.

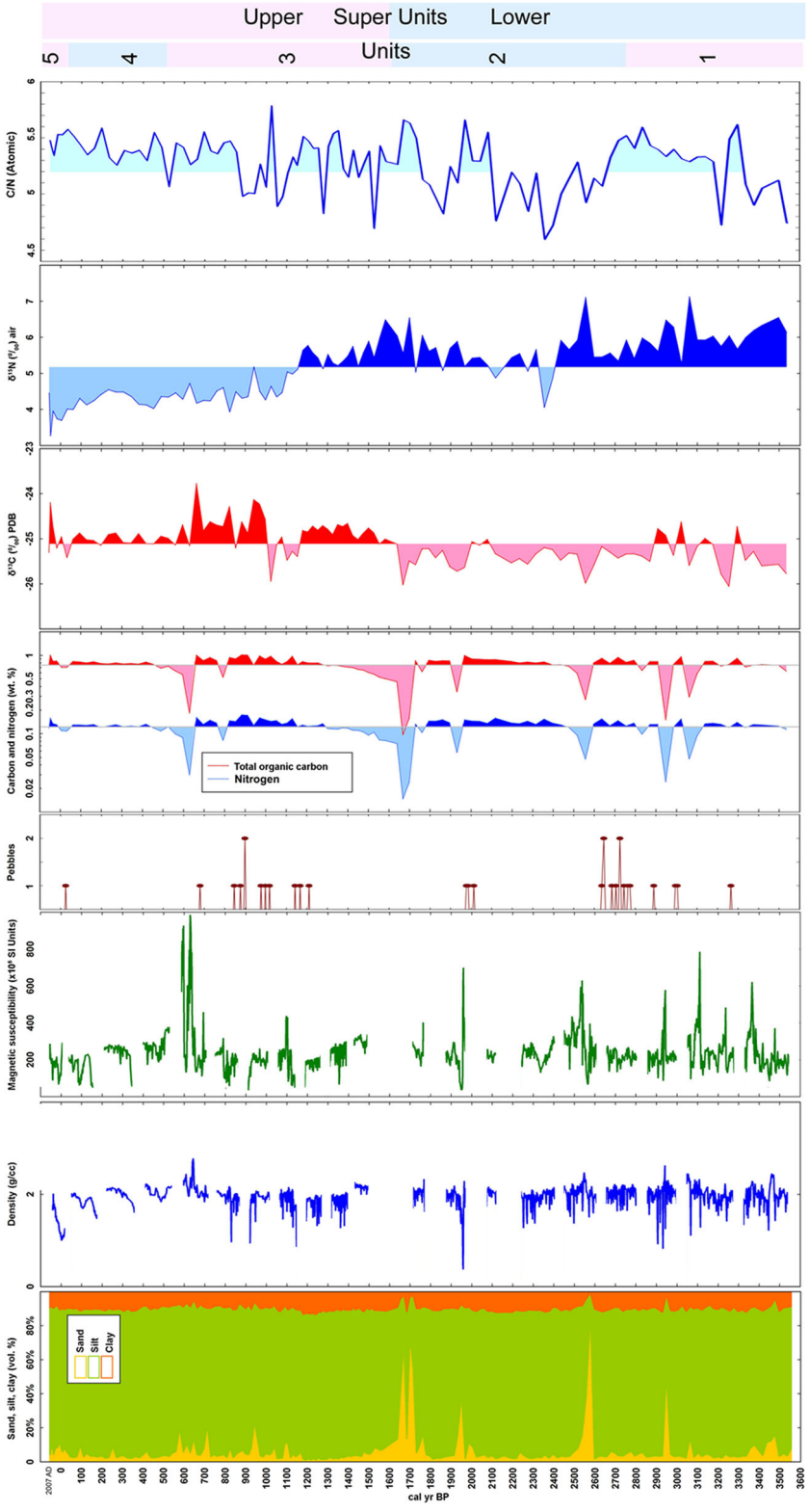

Fig. 5 Grain size (sand, silt, clay percentages), multi-sensor core logger data (density and magnetic susceptibility), pebble count, elemental and isotopic data (total organic carbon and nitrogen (wt.%), $\delta^{13}C$, $\delta^{15}N$ (‰) and the C/N atomic ratio) for units and super-units throughout JPC-24 plotted by age (cal yr BP).

Citation: *Polar Research* 2014, *33*, 17236, http://dx.doi.org/10.3402/polar.v33.17236

the average mean $\delta^{13}C$ and $\delta^{15}N$ values are -25 ‰ and 5‰, respectively, with ranges of ca. 2‰ ($\delta^{13}C$) and ca. 4‰ ($\delta^{15}N$). The lower super-unit covers the age range 3560–1600 cal yr BP, and the upper super-unit from 1600 cal yr BP–present. Average mean values for total organic carbon and nitrogen (wt.%) are 0.75 and 0.12, respectively, and the average mean atomic C/N ratio is 5.3. The upper super-unit has higher average mean values of total organic carbon and nitrogen (wt.%), and $\delta^{13}C$ that are higher than the mean average and lower $\delta^{15}N$ values. Comparison of the weight percentages and facies shows that the lowest values occur in coarser sediments. In contrast, the lower super-unit has average-mean isotopic signature values that are higher that the data set averages for $\delta^{15}N$, and lower for $\delta^{13}C$. Unit boundaries are defined by relatively small changes in the proxy data, resulting in less well-defined boundaries between units: 1/2, 3/4 and 4/5.

Units. Unit 1 (3560–2600 cal yr BP) is composed of hemipelagic sediment with some distal turbidites, and includes the highest sustained $\delta^{15}N$ values within this core, with values consistently above the data set mean average. Unit 2 (2600–1600 cal yr BP) is characterized by organic-rich hemipelagic sediment including three turbidites, and lower $\delta^{15}N$ values through the middle of the unit. Unit 3 (1600–500 cal yr BP) is dominated by organic-rich hemipelagic sediment and includes a layer of abundant angular granules interpreted as ice-rafted debris. The maximum $\delta^{13}C$ value, -24‰, occurs in unit 3 along with above average concentrations of carbon and nitrogen. Unit 4 (500–50 cal yr BP) is composed of low density, low magnetic susceptibility hemipelagic sediment, with no pebbles and less sand relative to the other units (vol.%). Throughout units 3 and 4, $\delta^{15}N$ decreases toward the core top, with a slight increase in $\delta^{15}N$ values in unit 4. Unit 5 is characterized by a wider range of $\delta^{15}N$ values and high $\delta^{13}C$ values (-24.2‰).

Discussion

The ratio of biogenic to terrigenous sediment determines the magnetic susceptibility character. High percentages of biogenic sediment result in relatively low magnetic susceptibility values, and high percentages of terrigenous sediment produce high magnetic susceptibility values. Consequently, magnetic susceptibility has been widely implemented as a proxy for the ratio of marine to land-derived sediment. From 1600 cal yr BP to present, low magnetic susceptibility is more frequent in the upper super-unit, and most probably represents an increase in the accumulation of marine organic matter at this time.

In glacimarine environments coarse sediments, grain size greater than 4 mm, are typically interpreted as ice-rafted debris. The importance of sea ice in the Bransfield Strait for sedimentation is well defined by extreme levels of seasonal variability in the particle flux. As much as 97–99% of the mass flux occurs during the austral summer (Wefer et al. 1988; Khim et al. 2005). Ice-rafted debris is delivered to the deep basin either by sea ice or by icebergs, meaning that it also requires open ocean conditions. Units 1 and 3 contain the highest pebble counts indicating a larger contribution of ice-rafted debris and also low magnetic susceptibility values. These proxies reveal the increased relative inputs of marine organic accumulation and terrigenous material from ice-rafted debris, not turbidites. The dominance of marine organic matter and ice-rafted debris in the sedimentary record establishes that open ocean conditions prevailed during those times. More restricted ice cover allows for more efficient dispersal of ice-rafted debris across the basin.

Most of the sediment in JPC-24 (90%) is homogeneous hemipelagic sediment with a mean average C/N ratio of 5.3. The results in this study show a very strong positive correlation (correlation coefficient of 0.98) between carbon and nitrogen with a very low standard deviation (0.04). We interpret these results to mean that the carbon and nitrogen isotopic signature represents marine organic matter. In Fig. 6 the best-fit line of the carbon and nitrogen data crosses the origin signifying that that these samples contain negligible amounts of inorganic carbon or nitrogen. The slope of the C/N ratio is 5.1, close to the stoichiometry found in the traditional Redfield Ratio (ca. 6.6 [Redfield 1934]). To achieve the Redfield Ratio marine organisms must achieve a balanced lifestyle requiring limiting nutrients and tolerable levels of environmental stress. When balance is not achieved the Redfield Ratio becomes a broader realm of C/N values between 3 and 8.75 (Jørgensen & Bendoricchio 2001). Phytoplankton attain the Redfield Ratio when growing at their maximum growth rate (Goldman et al. 1979) and if the supply of nutrients is sufficient that no single nutrient limits growth, then the only limitation of biomass is the quantity of nutrients available. From this data we infer that changes in the isotopic signature are likely to represent changes in surface biomass (productivity).

The carbon isotopic signature in our data has a mean average $\delta^{13}C$ value of -24 ‰ that can be explained by the sources and metabolic pathways used. Sources of carbon for marine phytoplankton are dissolved-marine bicarbonate with a $\delta^{13}C$ value of ca. 0‰ and dissolved CO_2 that has a $\delta^{13}C$ value of ca. -6‰ (Meyers 1994). Marine phytoplankton use the photosynthetic C3 pathway that creates an isotopic shift in of about -20‰, as a

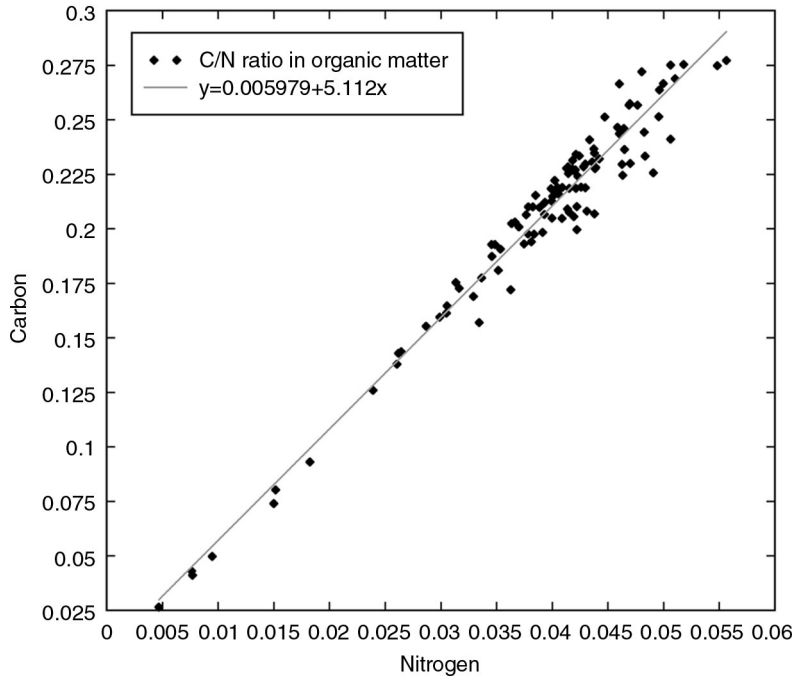

Fig. 6 Atomic carbon and nitrogen ratio of organic matter. The correlation coefficient for the best-fit line is 0.99. The traditional Redfield Ratio has a slope between 3 and 8 and here the best-fit line has a slope of 5.1.

function of dissolved CO_2, temperature, light and nutrient supply (Meyers 1997).

The trend toward higher $\delta^{13}C$ values in the younger parts of the core (Fig. 7) could be driven by the "cold-water effect" proposed by Rau et al. (1989) whereby increased isotopic discrimination toward ^{12}C occurs when the abundance of dissolved CO_2 increases. Additionally, the concentration of dissolved CO_2 is higher in cold water so it is preferentially incorporated during photosynthetic activity over marine bicarbonate. Light is also an important factor in surface waters and the amount of irradiance can influence $\delta^{13}C$ values; in laboratory experiments exposure to increased levels of irradiance over a 24-h period caused 1.5‰ higher $\delta^{13}C$ values in phytoplankton (Burkhardt et al. 1999). Changes in the environmental conditions are expected to be related to changes in diatom assemblages.

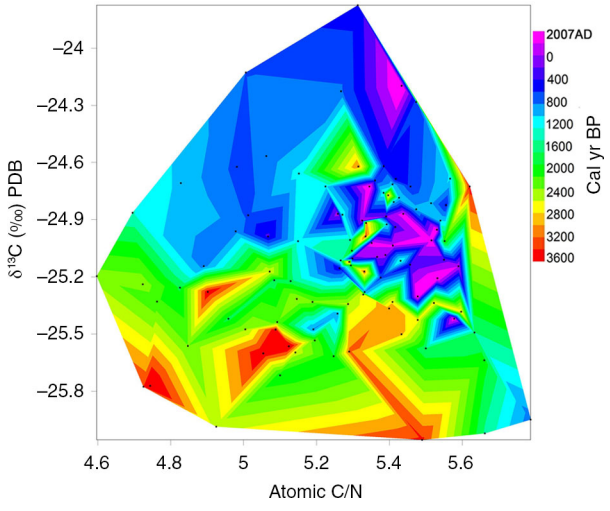

Fig. 7 Three-dimensional plot of $\delta^{13}C$ and C/N ratio. The highest $\delta^{13}C$ values occur in the youngest parts of the core.

Using a sedimentary record from the Central Bransfield Basin, Barcena et al. (1998) showed that there has been an increase in the amount of diatom sea-ice taxa over the last 2000 years. The range of carbon isotopic values changes quite dramatically during seasonal sea ice diatom taxa variations by up to 10‰ (Henley et al. 2012). Because our $\delta^{13}C$ values only change by 1–1.5‰, it is possible that only small modifications to the assemblages are driving the changes we observe. It is unlikely that our results represent transfer from autotrophic to heterotrophic communities because this would result in a step-wise enrichment of both $\delta^{15}N$ (3.5‰) and $\delta^{13}C$ (1.5‰) values (Rau et al. 1983; Minagawa & Wada 1984). It therefore seems reasonable to attribute the increase in $\delta^{13}C$ values at 1600 cal yr BP to changes in the environmental conditions that affected the diatom assemblages.

Using both the carbon and nitrogen isotopic signatures, plotted with the mass accumulation rate of organic matter, provides an insight into the ratio of productivity in surface waters to accumulation on the seafloor. Figure 8 shows

Citation: *Polar Research* 2014, *33*, 17236, http://dx.doi.org/10.3402/polar.v33.17236

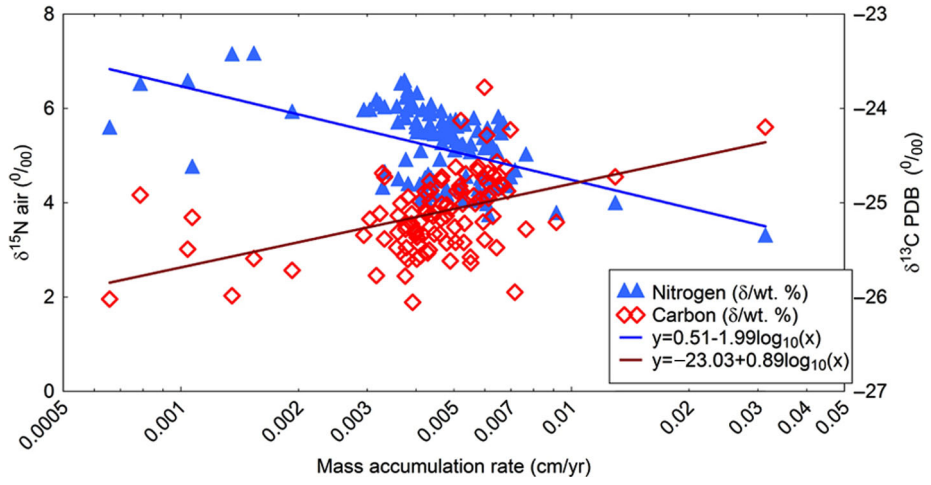

Fig. 8 Total organic carbon and nitrogen mass accumulation rate, $\delta^{13}C$ and $\delta^{15}N$ values cross-plot with best-fit lines, correlation coefficients for nitrogen 0.48 and carbon 0.41, standard deviation of 0.69 and 0.36, respectively.

that $\delta^{13}C$ and total organic carbon mass accumulation values have a positive relationship, whereas $\delta^{15}N$ values and nitrogen mass accumulation values have a negative relationship. This is further evidence that there is a strong relationship between the accumulation of organic matter in sediment and the isotopic signature. The organic matter provides a record of isotopic fractionation during primary production related to surface water processes.

The utilization of different nitrogen compounds in surface waters is controlled by the uptake of different compounds of nitrogen so the $\delta^{15}N$ signature changes as a function of the compound used. The mean average $\delta^{15}N$ of the marine organic matter in this core is 5‰, a value similar to that of nitrate entering the oceans via continental runoff (5–10‰). In the upper super-unit there is a trend towards lower $\delta^{15}N$ values. So long as the nutrient supply maintains an abundance of surface $^{14}[N]\text{-}NO_3^-$, increases in productivity result in lower $\delta^{15}N$ values than would be expected with increasing levels of productivity (Meyers 1997; Altabet & Francois 2001). Nutrient supply levels are so high in the Antarctic Peninsula region that they fuel not just local but also regional increases in productivity (Ardelan et al. 2010). In the Bransfield Strait during the austral summer, regenerated production using "recycled" ammonium with lower $\delta^{15}N$ values accounts for more than 80% of the total primary production (Koike et al. 1986). Regenerated production can also be fuelled by ammonium ($NH4^+$) produced by phytoplankton as a mechanism to lose excess energy gained from increased levels of irradiance (Lomas et al. 2000). Recent studies of the mixed layer depth and nitrate assimilation in the Southern Ocean strongly suggest that light limitation is the dominant control of nitrate assimilation (DiFiore et al. 2010). An increase in regenerated production could alter the $\delta^{15}N$ values in relative isolation from the $\delta^{13}C$ values resulting in a decoupled $\delta^{13}C$ and $\delta^{15}N$ signal.

Irradiance of surface waters causes increased late summer levels of regenerated production and can change the community structure. Differential uptake and remineralization following a seasonal pattern has also been observed (Lourey et al. 2003). Coincident maximums for both mass flux and regenerated production occur in the late summer. The concomitant increases in late summer (January–February) regenerated production and mass flux result in a greater preservation potential of the isotopic signature.

Correlation of units to Late Holocene climate periods

Climate records from the maritime western Antarctic Peninsula feature regional heterogeneity and the results in this paper allow new comparisons and correlation of Late Holocene climate changes to be made (Fig. 9). Unit 1 (3560–2600 cal yr BP) is broadly synchronous with the later stages of the Mid-Holocene Warm Period (Fig. 9), a period of warmth, reduced sea ice and greater melt-water-derived sedimentation (Bentley et al. 2009). The Mid-Holocene Warm Period is seen in many records from this region, ending in Palmer Deep at 3360 (Domack et al. 2001), in the Bransfield Strait (Heroy et al. 2008) and Maxwell Bay (Milliken et al. 2009; Majewski et al. 2012) at 2000–2600 cal yr BP, and in the Firth of Tay at 3500 cal yr BP (Michalchuk et al. 2009). Unit 2 (2600–1600 cal yr BP) is broadly synchronous with the Neoglacial Interval, a period of pronounced shift to colder climate on land and increased sea ice and cooler waters at

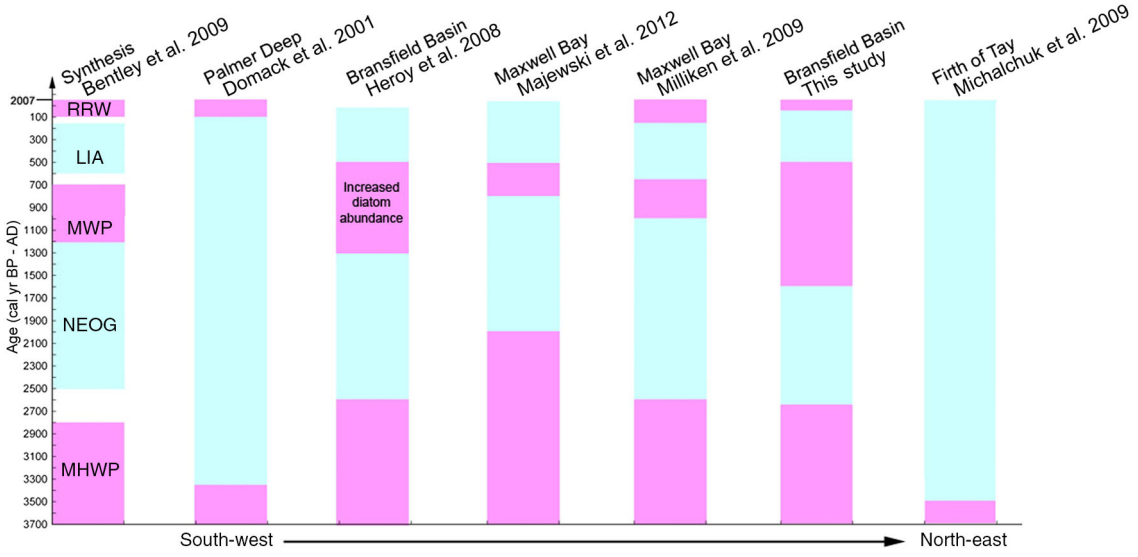

Fig. 9 Summary showing the warm (pink) and cold (blue) periods defined in other studies and compared to this study. Bentley et al. (2009) presented a summary including onshore and offshore work but the timings of the changes are uncertain and are shown as gaps. The other six columns are marine records organized geographically from south-west to north-east. Terms are abbreviated as follows: Recent Rapid Warming (RRW); Little Ice Age (LIA); Medieval Warm Period (MWP); Neoglacial (NEOG); Mid-Holocene Warm Period (MHWP).

sea (Bentley et al. 2009). Cores from the Palmer Deep (Domack et al. 2001) and Firth of Tay (Michalchuk et al. 2009) document the Neoglacial Interval as a period of cooling continuing through to the recent rapid warming (Fig. 9). Unit 3 (1600–500 cal yr BP) is broadly synchronous with the Medieval Warm Period (Bentley et al. 2009; Lu et al. 2012), observed in proxy data from Maxwell Bay (Milliken et al. 2009; Majewski et al. 2012), and the Bransfield Basin (Heroy et al. 2008 and this study). El Niño Southern Oscillation records peak at 1200 cal yr BP, providing a potential explanation for the greater variability in proxy data from this study at that time (Bentley et al. 2009). Other studies from the region also document increased sea-surface temperatures following 1600–2000 cal yr BP (Nielsen et al. 2004). Prior to 650 cal yr BP the climate warmed, shown by the fact that the Collins Ice Cap on King George Island was at or landward of its present extent (Hall 2007) and in the western Antarctic Peninsula ice extent was at or behind its present extent between 970 and 700 cal yr BP (Hall et al. 2010). Unit 4 (500–50 cal yr BP) is similar in timing to the Little Ice Age (Bentley et al. 2009; Lu et al. 2012), and also coincides with a decrease in productivity at the Palmer Deep (Sjunneskog & Taylor 2002). Land-based records show glacier advances at this time, for example the Collins Ice Cap advanced at 650 cal yr BP (Hall 2007). In Palmer Deep, the Little Ice Age is dated between 700 and 150 cal yr BP (Domack et al. 2001). Unit 5 (50 cal yr BP–present) is equivalent to the present-day recent rapid warming. It has been recognized in numerous proxy records by higher sedimentation rates, increased total organic carbon, more ice-rafted debris and higher clay percentages (Bentley et al. 2009; Lu et al. 2010). These diachronous Late Holocene climatic changes that coincide with the Neoglacial, Medieval Warm Period, Little Ice Age and Recent Rapid Warming highlight the importance of global climate to this region.

Summary and conclusions

This study defines two super-units and five units that are broadly synchronous with known climatic intervals across the Antarctic Peninsula region. An interval representing a climatic change is defined by the super-unit boundary at approximately 1600 cal yr BP. Since then, the climate in the Bransfield Strait has changed and these changes are recorded in diatom productivity proxies in the sediments. Correlation to other proxy records from the region (Domack et al. 2001; Heroy et al. 2008; Michalchuk et al. 2009; Milliken et al. 2009; Majewski et al. 2012) indicates that these Late Holocene changes are broadly synchronous, yet high-resolution studies are starting to show that each area has its own detailed history, unlike the changes happening across the Antarctic Peninsula today.

The integrated proxy data show that regional climatic changes, previously identified in more proximal locations, can be identified in Holocene sediments accumulating in

Citation: *Polar Research* 2014, *33*, 17236, http://dx.doi.org/10.3402/polar.v33.17236

the deep Bransfield Basin. This suggests that drill cores obtained from the Bransfield Basin in the future could be used to reconstruct older Late Quaternary glacial–interglacial cycles. Records from the key time periods include material derived from the glacimarine environment during glacial advances and retreats.

Detailed analysis of the geochemical data allows us to make some general conclusions about the marine environmental conditions at the time of deposition. Since 1600 cal yr BP, the isotopic signatures of carbon and nitrogen document a change in the surface water conditions that are recorded by the geochemical characteristics of the diatom assemblages. The similarity of the C/N ratio to the traditional Redfield Ratio indicates an autochthonous marine planktonic source for the organic matter unlimited by nutrients. Variations in the amount of organic matter in the sediment correlate well with changes in the isotopic signature, interpreted as a record of surface water biogeochemical fractionation. Seasonal maximums in organic matter reaching the basin floor and regenerated production during the summer sea ice free season provide a geochemical signature of the past environmental conditions. The changes observed were likely to have been driven by increases in surface water irradiance as the sea-ice season shortens.

Acknowledgements

We acknowledge the National Science Foundation for funding this project (OPP-0739596 to JSW and JBA). We thank the science party of NBP0703, Rice University Sedimentology Laboratory, Petroleum Systems and Geochemistry Program at the University of Houston, Steve Ackley for discussion of sea-ice trends, Qi Fu and three anonymous reviewers.

References

Altabet M.A. & Francois R. 2001. Nitrogen isotope biogeochemistry of the Antarctic Polar Frontal Zone at 170°W. *Deep-Sea Research Part II 48*, 4247–4273.

Anderson J.B. 1999. *Antarctic marine geology*. Cambridge: Cambridge University Press.

Ardelan M.V., Holm-Hansen O., Hewes C.D., Reiss C.S., Silva N.S., Dulaiova H., Steinnes E. & Sakshaug E. 2010. Natural iron enrichment around the Antarctic Peninsula in the Southern Ocean. *Biogeosciences 7*, 11–25.

Arndt J.E., Werner Schenke H., Jakobsson M., Nitsche F.O., Buys G., Goleby B., Rebesco M., Bohoyo F., Hong J., Black J., Greku R., Udintsev G., Barrios F., Reynoso-Peralta W., Taisei M. & Wigley R. 2013. The International Bathymetric Chart of the Southern Ocean (IBCSO) Version 1.0. A new bathymetric compilation covering circum-Antarctic waters. *Geophysical Research Letters 40*, 3111–3117.

Barcena M.A., Gersonde R., Ledesma S., Fabres J., Calafat A.M., Canals M., Sierro F.J. & Flores J.A. 1998. Record of Holocene glacial oscillations in Bransfield Basin as revealed by siliceous microfossil assemblages. *Antarctic Science 10*, 269–285.

Bentley M.J., Hodgson D.A., Smith J.A., O Cofaigh C., Domack E.W., Larter R.D., Roberts S.J., Brachfeld S., Leventer A., Hjort C., Hillenbrand C.D. & Evans J. 2009. Mechanisms of Holocene paleoenvironmental change in the Antarctic Peninsula region. *The Holocene 19*, 51–69.

Boldt K.V., Nittrouer C.A., Hallet B., Koppes M.N., Forrest B.K., Wellner J.S. & Anderson J.B. 2013. Modern rates of glacial sediment accumulation along a 15° S–N transect in fjords from the Antarctic Peninsula to southern Chile. *Journal of Geophysical Research—Earth Surface 118*, 2072–2088.

Burkhardt S., Riebesell U. & Zondervan I. 1999. Effects of growth rate, CO_2 concentration, and cell size on the stable carbon isotope fractionation in marine phytoplankton. *Geochimica et Cosmochimica Acta 63*, 3729–3741.

Carbotte S.M., Ryan W.B.F., O'Hara S., Arko R., Goodwillie A., Melkonian A., Weissel R.A. & Ferrini V.L. 2007. *Antarctic multibeam bathymetry and geophysical data synthesis: an on-line digital data resource for marine geoscience research in the Southern Ocean. U.S. Geological Survey Open-File Report 2007-1047. Short Research Paper 002*. Reston, VA: U.S. Geological Survey.

Cook A.J., Fox A.J., Vaughan D.G. & Ferrigno J.G. 2005. Retreating glacier fronts on the Antarctic Peninsula over the past half-century. *Science 308*, 541–544.

DiFiore P.J., Sigman D.M., Karsh K.L., Trull T.W., Dunbar R.B. & Robinson R.S. 2010. Poleward decrease in the isotope effect of nitrate assimilation across the Southern Ocean. *Geophysical Research Letters 37*, article no. L17601, doi: 10.1029/2010GL044090.

Domack E., Leventer A., Dunbar R., Taylor F., Brachfeld S. & Sjunneskog C. 2001. Chronology of the Palmer Deep site, Antarctic Peninsula; a Holocene paleoenvironmental reference for the circum-Antarctic. *The Holocene 11*, 1–9.

Ducklow H.W., Baker K., Fraser W.R., Martinson D.G., Quetin L.B., Ross R.M., Smith R.C., Stammerjohn S. & Vernet M. 2007. Marine pelagic ecosystems: the West Antarctic Peninsula. *Philosophical Transactions of the Royal Society of London B 362*, 67–94.

García M., Ercilla G., Anderson J.B. & Alonso B. 2008. New insights on the post-rift seismic stratigraphic architecture and sedimentary evolution of the Antarctic Peninsula margin (Central Bransfield Basin). *Marine Geology 251*, 167–182.

Goldman J.C., McCarthy J.J. & Peavey D.G. 1979. Growth rate influence on the chemical composition of phytoplankton in oceanic waters. *Nature 279*, 210–215.

Griffith T.W. & Anderson J.B. 1989. Climatic control of sedimentation in bays and fjords of the northern Antarctic Peninsula. *Marine Geology 85*, 181–204.

Hall B.L. 2007. Late-Holocene advance of the Collins Ice Cap, King George Island, South Shetland Islands. *The Holocene 17*, 1253–1258.

Hall B.L., Koffman T. & Denton G.H. 2010. Reduced ice extent on the western Antarctic Peninsula at 700–900 cal yr BP. *Geology 38*, 635–638.

Henley S.F., Annett A.L., Ganeshram R.S., Carson D.S., Weston K., Crosta X., Tait A., Dougans J., Fallick A.E. & Clarke A. 2012. Factors influencing the stable carbon isotopic composition of suspended and sinking organic matter in the coastal Antarctic sea ice environment. *Biogeosciences 9*, 1137–1157.

Heroy D. & Anderson J.B. 2005. Ice sheet extent on the Antarctic Peninsula during the last glacial maximum (LGM)—insights from glacial geomorphology. *Geological Society of America Bulletin 117*, 1497–1512.

Heroy D.C. & Anderson J.B. 2007. Radiocarbon constraints on Antarctic Peninsula ice sheet retreat following the Last Glacial Maximum (LGM). *Quaternary Science Reviews 26*, 3286–3297.

Heroy D.C., Sjunneskog C. & Anderson J.B. 2008. Holocene climate change in the Bransfield Basin, Antarctic Peninsula; evidence from sediment and diatom analysis. *Antarctic Science 20*, 69–87.

Jørgensen S.E. & Bendoricchio G. 2001. *Fundamentals of ecosystem modeling*. Amsterdam: Elsevier.

Khim B.K., Kim D., Shin H.C. & Kim D.Y. 2005. Stable carbon and nitrogen isotopes of sinking particles in the eastern Bransfield Strait (Antarctica). *Ocean Science Journal 40*, 167–176.

Koike I., Holm-Hansen O. & Biggs D.C. 1986. Inorganic nitrogen metabolism by Antarctic phytoplankton with special reference to ammonium cycling. *Marine Ecology Progress Series 30*, 105–116.

Lomas M.W., Rumbley C.J. & Glibert P.M. 2000. Ammonium release by nitrogen sufficient diatoms in response to rapid increases in irradiance. *Journal of Plankton Research 22*, 2351–2366.

Lourey M.J., Trull T.W. & Sigman D.M. 2003. Sensitivity of $\delta^{15}N$ of nitrate, surface suspended and deep sinking particulate nitrogen to seasonal nitrate depletion in the Southern Ocean. *Global Biogeochemical Cycles 17*, 1–7.

Lu Z., Rickaby R.E.M., Kennedy H., Kennedy P., Pancost R.D., Shaw S., Lennie A., Wellner J. & Anderson J.B. 2012. An ikaite record of late Holocene climate at the Antarctic Peninsula. *Earth and Planetary Science Letters 325–326*, 108–115.

Lu Z., Rickaby R.E.M, Wellner J., Georg B., Charnley N., Anderson J.B. & Hensen C. 2010. Pore fluid modeling approach to identify recent meltwater signals on the west Antarctic Peninsula. *Geochemistry, Geophysics, Geosystems 11*, 14–21.

Majewski W., Wellner J.S., Szczuciński W. & Anderson J.B. 2012. Holocene oceanographic and glacial changes recorded in Maxwell Bay, West Antarctica. *Marine Geology 326–328*, 67–79.

Meredith M.P. & King J.C. 2005. Rapid climate change in the ocean west of the Antarctic Peninsula during the second half of the 20th century. *Geophysical Research Letters 32*, article no. L19604, doi: 10.1029/2005GL024042.

Meredith M.P., Wallace M.I., Stammerjohn S.E., Renfrew I.A., Clarke A., Venables H.J., Shoosmith D.R., Souster T. & Leng M.J. 2010. Changes in the freshwater composition of the upper ocean west of the Antarctic Peninsula during the first decade of the 21st century. *Progress in Oceanography 87*, 127–143.

Meyers P.A. 1994. Preservation of elemental and isotopic source identification of sedimentary organic matter. *Chemical Geology 114*, 289–302.

Meyers P.A. 1997. Organic geochemical proxies of paleoceanographic, paleolimnologic, and paleoclimatic processes. *Organic Geochemistry 27*, 213–250.

Michalchuk B.R., Anderson J.B., Wellner J.S., Manley P.L., Majewski W. & Bohaty S. 2009. Holocene climate and glacial history of the northeastern Antarctic Peninsula: the marine sedimentary record from a long SHALDRIL core. *Quaternary Science Reviews 28*, 3049–3065.

Milliken K.T., Anderson J.B., Wellner J.S., Bohaty S.M. & Manley P.L. 2009. High-resolution climate history of Maxwell Bay, South Shetland Islands, Antarctica. *Geological Society of America Bulletin 121*, 1711–1725.

Minagawa M. & Wada E. 1984. Stepwise enrichment of 15N along food chains: further evidence and the relation between $\delta^{15}N$ and animal age. *Geochimica et Cosmochimica Acta 48*, 1135–1140.

Mulvaney R., Abram N.J., Hindmarsh R.C.A., Arrowsmith C., Fleet L., Triest J., Sime L.C., Alemany O. & Foord S. 2012. Recent Antarctic Peninsula warming relative to Holocene climate and ice-shelf history. *Nature 489*, 141–145.

Nielsen S.H.H., Koc N. & Crosta X. 2004. Holocene climate in the Atlantic sector of the Southern Ocean: controlled by insolation or oceanic circulation? *Geology 4*, 317–320.

Prezelin B.B., Hofmann E.E., Mengelt C. & Klinck J.M. 2000. The linkage between Upper Circumpolar Deep Water (UCDW) and phytoplankton assemblages on the west Antarctic Peninsula continental shelf. *Journal of Marine Research 58*, 165–202.

Rau G.H., Mearns A.J., Young D.R., Olson R.J., Schafer H.A. & Kaplan I.R. 1983. Animal $^{12}C/^{13}C$ correlates with trophic level in pelagic food webs. *Ecology 64*, 1314–1318.

Rau G.H., Takahashi T. & Des Marais D.J. 1989. Latitudinal variations in plankton $\delta^{13}C$: implications for CO_2 and productivity in past oceans. *Nature 341*, 516–518.

Redfield A.C. 1934. On the proportions of organic derivatives in seawater and their relation to the composition of plankton. In R.J. Daniel (ed.): *James Johnson memorial volume*. Pp. 177–192. Liverpool: Liverpool University Press.

Reynolds J.M. 1981. The distribution of mean annual temperatures in the Antarctic Peninsula. *British Antarctic Survey Bulletin 54*, 123–133.

Simms A.R., Milliken K.T., Anderson J.B. & Wellner J.S. 2011. The marine record of deglaciation of the South Shetland

Islands, Antarctica since the Last Glacial Maximum. *Quaternary Science Reviews 30*, 1538–1601.

Sjunneskog C. & Taylor F. 2002. Postglacial marine diatom record of the Palmer Deep, Antarctic Peninsula (ODP Leg 178, Site 1098) 1. Total diatom abundance. *Paleoceanography 17*, article no. 8003, doi: 10.1029/2000PA000563.

Steig E.J., Schneider D.P., Rutherford S.D., Mann M.E., Comiso J.C. & Shindell D.T. 2009. Warming of the Antarctic ice-sheet surface since the 1957 International Geophysical Year. *Nature 457*, 459–462.

Stuiver M., Reimer P.J. & Reimer, R. W. 2005. Calib v.6.0. Accessed on the internet at http://calib.qub.ac.uk/calib/ on 1 November 2008.

Taylor F. & Sjunneskog C. 2002. Postglacial marine diatom record of the Palmer Deep, Antarctic Peninsula (ODP Leg 178, Site 1098) 2. Diatom assemblages. *Paleoceanography 17*, article no. 1026, doi: 10.1029/2000PA000564.

Turner J., Colwell S.R., Marshall G.J., Lachlan-Cope T.A., Carleton A.M., Jones P.D., Lagun V., Reid P.A. & Iagovkina S. 2005. Antarctic climate change during the last 50 years. *International Journal of Climatology 25*, 279–294.

Vaughan D.G. & Doake C.S.M. 1996. Recent atmospheric warming and retreat of ice shelves on the Antarctic Peninsula. *Nature 379*, 328–379.

Wefer G., Fischer G., Fuetterer D. & Gersonde R. 1988. Seasonal particle flux in the Bransfield Strait, Antarctica. *Deep Sea Research Part I 35*, 891–898.

Willmott V., Rampen S.W., Domack E.W., Canals M., Damste J.S.S. & Schouten S. 2009. Holocene changes in Probiscia diatom productivity in shelf waters of the northwestern Antarctic Peninsula. *Antarctic Science 22*, 3–10.